Numerical Optimization of Flow Field Pattern by Mass Transfer and Electrochemical Reaction Characteristics in Proton Exchange Membrane Fuel Cells

Bonghwan Lee, Kiwon Park and Hyung-Man Kim[*]

Department of Mechanical Engineering & High Safety Vehicle Core Technology Research Center, INJE University, 607 Eobang-dong, Gimhae-si, Gyongsangnam-do 621-749, Republic of Korea
[*]E-mail: mechkhm@inje.ac.kr

Flow field pattern affects the mass transfer and electrochemical reaction characteristics which influence the distribution of reacting gases as well as the performance of proton exchange membrane fuel cell. The mass transfer caused by diffusion and convection can be optimized by designing a suitable flow field pattern for the proton exchange membrane fuel cell. To obtain a superior flow field pattern, we investigate numerically the internal mass transport and electrochemical reaction behaviors of the fuel cell with the single serpentine, the single parallel, the interdigitated and the pin flow field patterns. These results show that when the active area and operating conditions are identical, the single serpentine flow field pattern shows the best characteristics or similar characteristics to the interdigitated flow field pattern which shows the water accumulation because of the electrochemical reaction in the outlet region. However, the pin and the single parallel flow field patterns show the worst mass transfer characteristics, respectively because of the flooding and drying of membrane caused by uneven flow circulation.

1. INTRODUCTION

Proton exchange membrane fuel cells (PEMFCs) offer a promise of cleaner electricity that gives less impact on the environment than the traditional energy conversion technologies. To produce electricity efficiently, the reactants of hydrogen and oxygen must be uniformly supplied to promote mass transfer, and at the same time, the product water produced by electrochemical reaction must be constantly discharged to avoid performance loss. Direct electrochemical fuels, particularly hydrogen, provide the promise of being one of several possible long-term approaches to the improvement of

energy efficiency, energy sustainability, energy security, greenhouse gases reduction and global environmental conservation [1-6].

The optimizations of mass transfer and electrochemical reaction characteristics by changing the flow field patterns have been reported in the literature: Many papers have been dedicated to study the mentioned phenomenon, which is due to several reasons. Bautista-Rodríguez et al. [7] performed the study of design engineering, building and characterization of a PEMFC. The designs of polar plates and support plates are shown, in addition to polarization curves in order to determine the PEMFC performance at different cathodic pressures and types of flow in the system, co-current and counter current. Some studies were focused on the effects of active area size on steady-state characteristics of a working PEMFC with parallel, interdigitated, and serpentine flow channel design [8] and compared the transient characteristics of parallel and interdigitated flow fields [9]. To determine whether insufficient mass transfer can lead to performance loss, it is necessary to confirm that the concentration of reactants and products is not determined at the entrance of the fuel cell but at the catalyst layer (CL) which determines the performance of PEMFC. Depletion of reactants or accumulation of products at the catalyst layer causes loss of mass transfer detrimental to the performance. At the areas where the gases with polarities are lacking, irreversible membrane damages can occur locally, and it can lead to corrosion and performance degradation of the material [10].

Models play an important role in fuel cell development. PEM fuel cells use hydrogen as fuel and air as oxidizer. In PEMFC stack oxygen and hydrogen are consumed, and water and heat are generated. Humidification system is used to maintain hydration of the polymer membrane and to balance consumed water in the system [11-14]. Fuel cell flow channel scaling behavior was investigated for three different flow pattern archetypes (interdigitated, serpentine, and spiral interdigitated) by employing computational fluid dynamics (CFD). The range of investigation covered flow channels of macro feature size (> 500 μm) to micro feature size (< 100 μm), thereby each flow pattern archetype exhibits unique scaling behavior.

In the previous study, we proposed a systematic design process for the serpentine flow field to enhance the performance of PEMFC through a detailed parametric study on each of the three different channel heights and widths [15-17]. A new serpentine flow field with sub-channels and by-passes incorporated the experiments and the simulations to provide a better understanding and utilization of under-rib convective flow. If reacting gases flow in the same direction as the neighboring main channels, the under-rib convective flow were converged from the main channels to the sub-channels which not only reduces pressure drop but also enhances uniform gas supply and water diffusion. The maximum current and the power densities of the serpentine flow field with sub-channels and by-passes were increased by 18.85% and 23.74%, respectively, due to the promotion of under-rib convection than a conventional advanced serpentine flow field. It is necessary to minimize the activation loss region, the ohmic resistance loss region and the mass transport loss region up to the level of open circuit voltage (OCV).

The flow field design in the bipolar plates (BPs) is very difficult because the phenomena of mass transport and electrochemical reactions are so complicated that the contributions of each parameter to the performance of a real PEMFC cannot be measured separately. Because the mass transport behavior of hydrogen and oxygen gases under the ribs and in the channels of flow-pattern is

hardly observable empirically, numerical calculation is important for designing efficient flow fields suitable for the PEMFC stack. In this study, we studied the internal mass transport behavior numerically in four different flow-patterns of single serpentine flow field pattern (SSFFP), single parallel flow field pattern (SPFFP), interdigitated flow field pattern (IFFP) and pin flow field pattern (PFFP).

2. NUMERICAL MODEL

Table 1. Inlet at the anode and the cathode, operating conditions and geometry details of four flow field patterns, that is, SSFFP, SPFFP, IFFP and PFFP.

Inlet conditions	Anode		Cathode	
Gas	Hydrogen		Air	
Stoichiometry	1.5		2.0	
Inlet temperature (°C)	75		76	
Inlet relative humidity (%)	100		100	
Mass fraction of hydrogen	0.078		-	
Mass fraction of oxygen	-		0.169	
Mass fraction of water	0.561		0.274	
Operating conditions				
Exit pressure (kPa)	101			
Open circuit voltage (V)	0.96			
Cell temperature (°C)	75			
Flow field patterns	SSFFP	SPFFP	IFFP	PFFP
Channel width (mm)	1.0			-
Channel height (mm)	0.5			
Rib width (mm)	1.0			1.0 [a]
Surface area (mm^2), channel / rib	337 / 288	349 /276	336 / 289	442.7 / 182.3
MEA thickness (μm) [b]	50			
MEA thermal conductivity (W/m K)	0.15			
GDL thickness (μm)	250			
GDL permeability (m^2)	1.0E-12			
GDL porosity	70			
GDL thermal conductivity (W/m K)	0.21			

[a] pin diameter

[b] including 12.5 μm thickness of catalyst layer

The numerical analysis was based on a steady state three dimensional CFD model of a PEMFC. CFD programs based on STAR-CD version 4.12, a commercial finite volume technique solver, and ES-PEMFC version 2.40, an add-on tool modulated to PEMFCs, were used to solve the fully coupled governing equations. The model assumes a steady state, ideal gas properties, and homogeneous two phase flows. The computational domain for CFD-based PEMFC simulation consists of the anode gas channel, the anode gaseous diffusion layer, the membrane electrode assembly (MEA) layer, the

cathode gaseous diffusion layer, the cathode gas channel and the BP. The MEA is sandwiched between anode and cathode gaseous diffusion layers (GDL) which have a porous structure, and has a membrane and two electrodes comprised of highly dispersed carbon supported platinum catalysts. Table 1 lists the geometry details and properties of current collector, GDL and MEA, and Fig. 1 shows the four flow field patterns of the SSFFP, the SPFFP, the IFFP and the PFFP having the same reaction area of 6.25 cm^2.

| (a) SSFFP | (b) SPFFP |
| (C) IFFP | (d) PFFP |
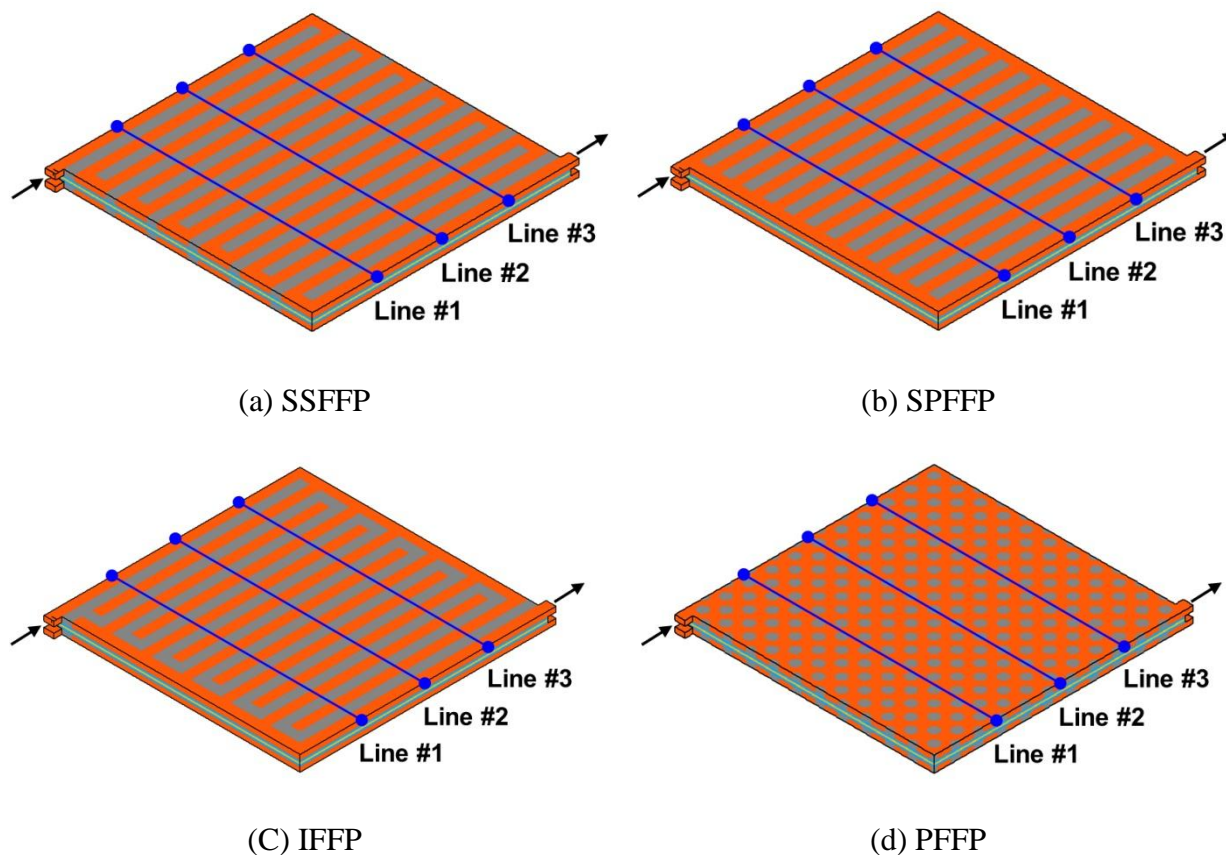
Figure 1. Schematics and locations of the four flow field patterns with active area of 6.25 cm^2 (2.5 cm × 2.5 cm) for profiling the performance related parameters.

The total number of the mesh was 1.50 million cells for the SSFFP, the SPFFP, and the IFFP, and 1.68 million cells for the PFFP, respectively. To verify the accuracy of the analysis, the sensitivity of the calculated mesh and the analysis results was verified by using 25cm^2 serpentine PEMFC [15]. The convergence residual of this analysis amounts to less than 1.0E-7, and the calculation was iterated for a maximum of 2000 times under the condition of convergence decision of less than 1% on the imbalance of chemical species such as hydrogen, oxygen, and water.

The operation conditions of PEMFC are largely classified into stoichiometric number (or flow rate), working pressure, humidification condition, and cell temperature, and they were used as one of

the variables to decide the performance of PEMFC. In this study, the inlet flow rate was fixed at 1.5 in the anodes and at 2.0 in the cathodes on the basis of the stoichiometric numbers. The parametric studies of four flow field patterns were conducted all under the same operating conditions as listed in Table 1. The numerical modeling is based on a single-domain formulation. The conservation equations are solved for mass, momentum, species, energy, and charge with electrochemical reactions. Assuming that liquid film is formed on the electrode surface during liquid water condensation, the Henry's law of solubility of gases in the liquid water is used to calculate the diffusion flux, electro-osmotic drag force, and water back diffusion [15,17].

3. RESULTS AND DISCUSSION

The performance of PEMFC was analyzed by using the present numerical model of the electrochemical reaction and transport phenomena which are fully coupled with the equations [17-18]. Therefore, the distributions of performance-related parameters are profiled and compared quantitatively at the same locations of line #1, #2 and #3 as shown in Fig. 1. The performance-related parameters include the partial pressure, hydrogen and oxygen mass fraction, liquid water mass fraction, temperature, membrane water content and net water flux per proton, and current density. They are investigated to generate the optimum flow field pattern that enhances the performance of PEMFC.

3.1 Anode and cathode pressure drops
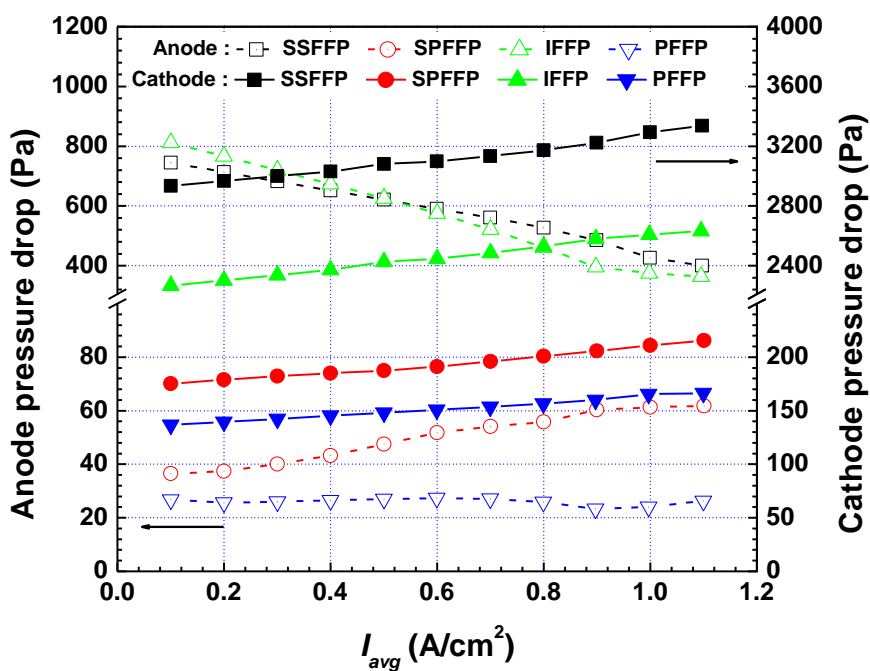
Figure 2. Variations of average anode (hollow symbol) and cathode (solid symbol) pressure drops with the average current density (I_{avg}) for four different flow field patterns.

The mass transfer generated inside the channel is explained with the following three mutually related descriptions: (1) changes in water content of membrane (λ) when products generated by the mass transfer and electrochemical reaction of reacting gas flow are hydrated at the membrane of electrolyte, (2) changes in net water flux per proton (α) that are caused by products generated by electrochemical reactions due to pressure differences between the anode and the cathode, and (3) temperature changes in the electrolyte membrane due to the behavior of the liquid water inside the channel. If the reactants at the anode and at the cathode are supplied with hydrogen and air, then it is self evident that during PEMFC operation there will be slight reductions in the concentrations of the hydrogen and the oxygen in the region of the electrode, respectively. The extent of change in concentration will depend on the current being taken from the fuel cell and on physical factors relating to how well the reactants can supply as well as how quickly the reactants can be replenished. These changes in concentration will cause drops in the partial pressures of the hydrogen and the oxygen. The reduction in the partial pressures of the reactants results in the performance degradation of PEMFC [19].

For a quantitative comparison among flow field patterns, the average values of activation areas are marked for the average current densities ranging from 0.1 to 1.1 A/cm^2 at an interval of 0.1 A/cm^2. Fig. 2 shows that as the average current density increases, the hydrogen mass fraction decreases due to the hydrogen oxidation reaction (HOR), and accordingly, the anode pressure drop decreases and the cathode pressure drop increases because of the internal products of the channel that disturbs the flow of reaction gas. However, in the anode pressure drop of the SPFFP, the pressure increases as the current density increases. This phenomenon can be explained by the distribution of cathode liquid water mass fractions shown in Fig. 3 (Section 3.2).

Manso et al. [20] reported the pressure drop characteristics of the most settings in PEMFC: serpentine, straight parallel, interdigited and pin (or mesh) flow fields. The straight parallel version is the simplest one requiring the smallest pressure drop by equally distributing the flow rate into many parallel paths. However, if the flow resistance is not maintained at the same level in each parallel flow channel a non-uniform distribution of the reactants may occur. The pin-type flow field consists of columnar pins arranged in a regular pattern. As the reactants flow through a network of series and parallel flow paths only low pressure drops occur. However, this leads to inhomogeneous gas distribution or reactant maldistribution and locally flooding and heating phenomenon. The role of under-rip convection in PEMFC with multi-pass serpentine flow fields (MPSFFs) was also numerically studied by Nam et al. [21]. The results showed that the enhanced under-rib convection in MPSFFs decreases the pressure drop across PEMFCs, which also contributes to the performance by reducing the power consumption.

3.2 Cathode liquid water mass fraction

Fig. 3 shows the distributions of the cathode liquid water mass fraction with the four flow field patterns. In the cases of the SPFFP shown in Fig. 3 (b), the liquid water mass fractions increased from 14% to 31% compared to the other flow field patterns as shown in Fig. 3 (a), (c) and (d). This is what

degrades the performance of the entire fuel cell by causing a flooding phenomenon due to the imbalance of the internal flow of the channel.

(a) SSFFP   (b) SPFFP

(C) IFFP   (d) PFFP
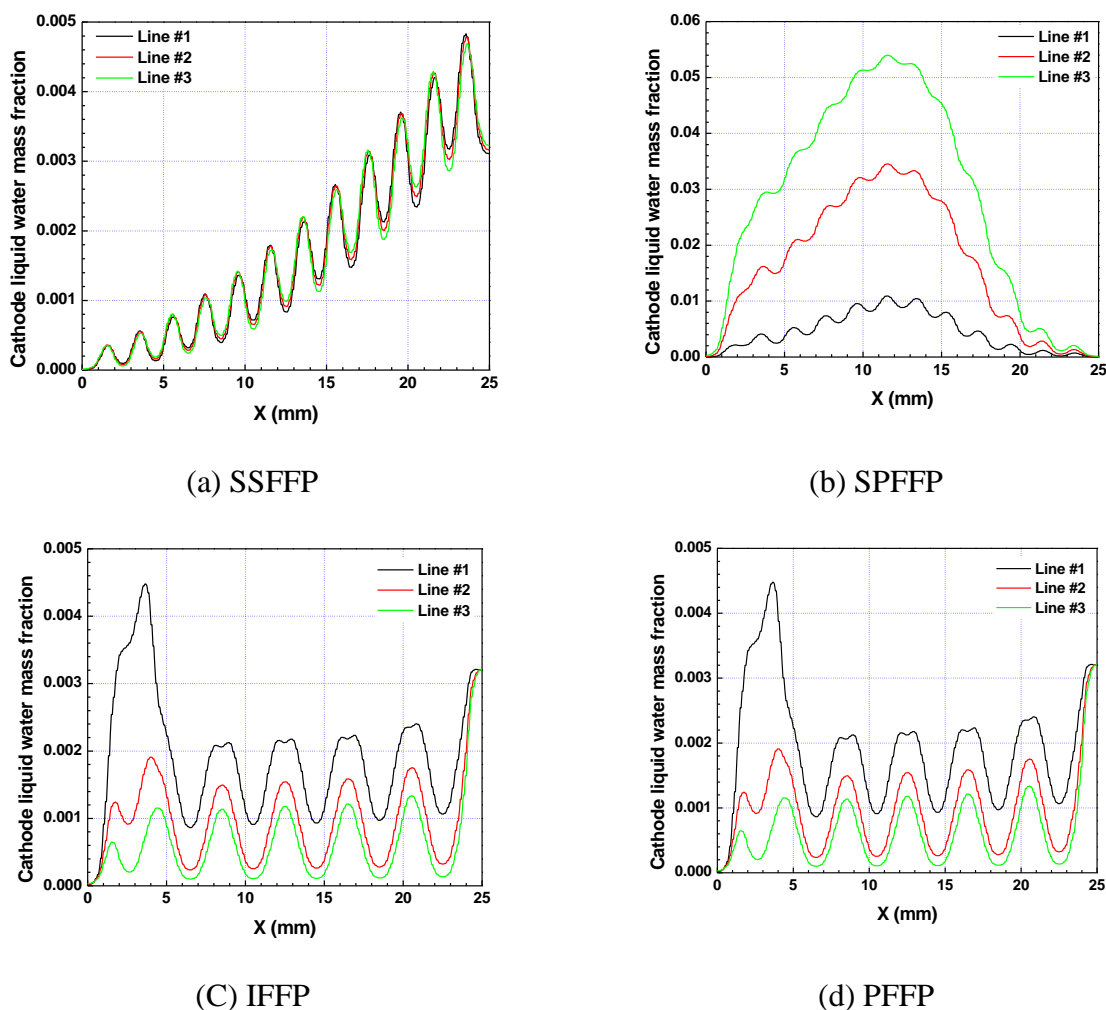
Figure 3. Comparison of the cathode liquid water mass fraction plots along profiling locations (line #1, #2, and #3) between the four different flow field patterns at $I_{avg} = 0.6$ A/cm^2.

Using a three-dimensional numerical model of the PEMFCs with conventional flow field, the distributions of velocity, oxygen mass fraction, current density, liquid water, and pressure were presented by Jang et al. [22]. It is found that without the corner design in the parallel flow field, the porous material is badly blocked by the liquid water, which leads to a high drop of liquid water in the fuel cell. It is also shown that the amount of liquid water of the serpentine flow field is the least among the three designs. The main reason is that the serpentine flow field has the highest flow speed for each channel, stronger convection in the flow field, which helps to remove the liquid water.

As for the PFFP that hardly undergoes pressure changes on the anode side, low pressure drops on cathode sides enhance water dispersion forces with the liquid water mass fraction approaching to 0 in the section where $X \approx 0{\sim}15$ mm, whereas on the wall around the outlet ($X \approx 20{\sim}25$ mm) the driving

force of the reaction gas inside the channel reduces ending up in flow imbalance and water congestion phenomena.

One of the main concerns of the BPs designers is to prevent the flooding effect in the cathode. Therefore, the application of different geometries in the anodic and cathodic sides of the PEMFC is advisable. Generally, geometries with higher pressure drop of serpentine and interdigitated flow fields that enhance convective flow are used for the cathode, because they help to eliminate excess water, also improving the efficiency of the electrochemical reaction [20].

3.3 MEA surface temperature

The surface temperatures of the cathode MEA for each profiling location are shown in Fig. 4 at I_{avg} = 0.6 A/cm^2. The temperature of each flow field pattern increases with the current density increase, which is due to the high reaction rate. The electrochemical reactions inside PEMFC are mainly the exothermic reactions and the reactions of cathodes appear to be higher than those of anodes. Like the boundary condition presented in Table 1, the numerical model built here at 75 °C of the well temperature boundary condition shows significant temperature changes on the anode and cathode MEA surfaces on account of the product water accumulated inside the channel. The water inside the channel is to cool down the reaction heat.

The temperature of the SPFFP in Fig. 4 (b) reaches approximately to 75.9 °C, which is close to the initial reaction gas temperature of 75 °C due to the cooling effect in the section where $X \approx 4{\sim}19$ mm and the water content becomes maximal. By contrast, the temperature soars up to 98.3 °C resulting from lack of water in the section where $X \approx 0$ mm, 25 mm and the water content is very low. Similar results are found in the PFFP in Fig. 3 (d), where the temperature ranges from 78.9 °C to 83.4 °C in the section that $X \approx 0{\sim}15$ mm.
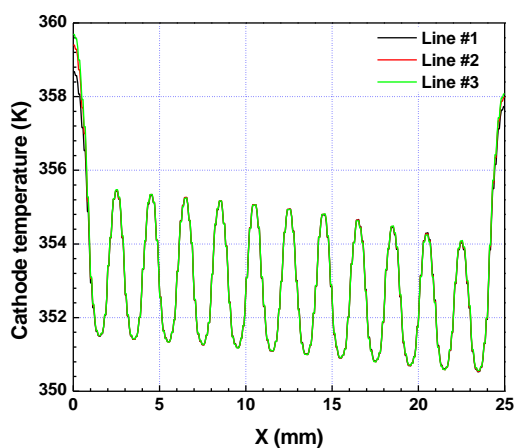
(a) SSFFP
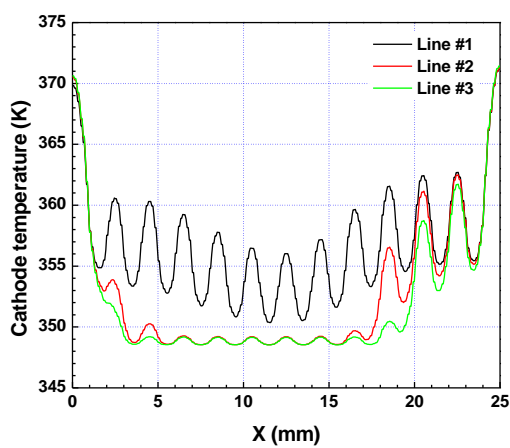
(b) SPFFP

(C) IFFP   (d) PFFP
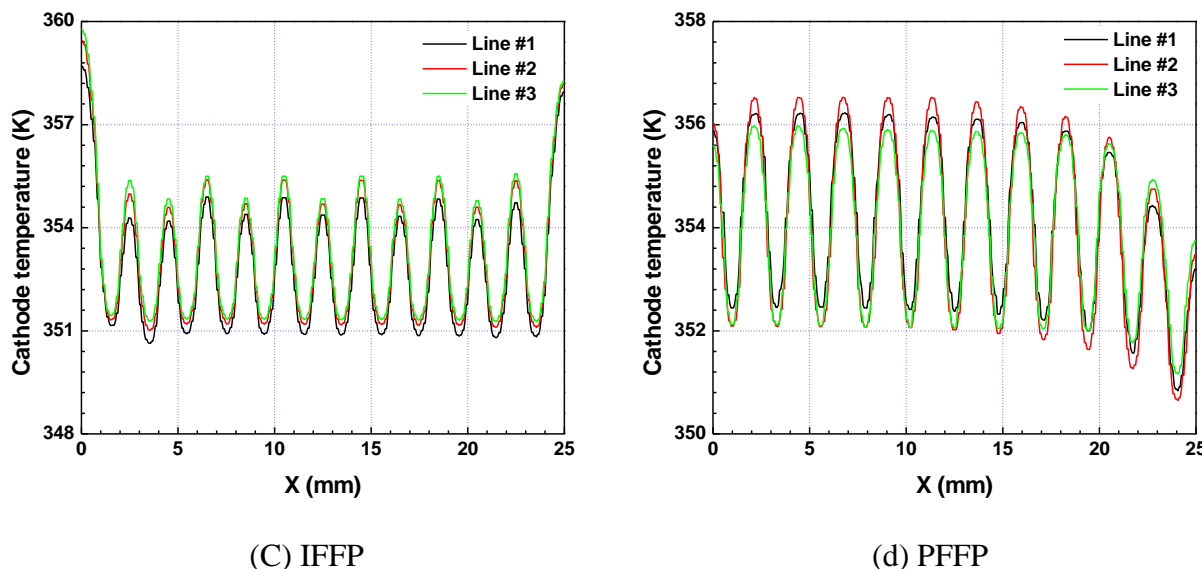
Figure 4. Comparison of the cathode temperature plots along profiling locations (line #1, #2, and #3) between the four different flow field patterns at I_{avg} = 0.6 A/cm^2.

As for the SSFFP and the IFFP in Fig. 3(a) and (b), cathode liquid water mass fraction is distributed within a similar range that the temperature distribution from the inlet to outlet is uniform particularly in the IFFP, while it gets lower near the outlet in the SSFFP.

Hwang [23] analysed the influence of the of operation temperature on the performance of the PEMFC using plates with 25 cm^2 of active area, with single serpentine type flow fields, in which the channel to rib width ratio remained constant. Water management in the polymeric electrolyte membrane is essential to obtain the maximum power of a PEM type fuel cell as a complete hydration is required to allow good proton conduction. However, for low temperatures PEMFC and under certain operating conditions; high humidification of the reactants, and high current densities, the gases inside the cells become oversaturated with water vapor which may condense in the cathode side, resulting in a lower power output. Hydration of the MEAs can be achieved by moisturizing the reactive flows. On the other hand, water is generated internally at the cathode side as a result of the electrochemical reaction.

3.4 Membrane water content

PEM fuel cell membrane assumes hydrophilic property to maintain water content (λ), and as in Fig. 4(a), water content (λ) and membrane conductivity (σ_m) have a proportional linear relationship [24-25]. Fuller, *et al.* [26] published that a completely hydration took place when the maximal value of λ was 14. Membrane water content is determined by water activity (a_k) in Eqs. (1) - (3) and becomes a major determinant for the membrane conductivity as follows [15,18]:

$$\lambda = 0.043 + 17.81a_k - 39.85a_k + 36a_k^3 \quad (0 \leq a_k \leq 1)$$
$$= 14 + 1.4(a_k - 1) \qquad\qquad (1 \leq a_k \leq 3)$$

(1)

$$a_k = \frac{X_{w,k} P(x,y)}{P_{w,k}^{sat}} \tag{2}$$

$$\sigma_m = (0.514\lambda - 0.326)\exp\left[1268\left(\frac{1}{303} - \frac{1}{T(x,y)}\right)\right] \tag{3}$$

Where $P_{w,k}^{sat}$ is the vapor pressure of water in stream k, $X_{w,k}$ the mole fraction of water in stream k, $P(x,y)$ is the pressure in Pa and $T(x,y)$ is the diffusion temperature in K. As shown in Fig. 5, when the average membrane water content and the average membrane conductivity are compared in an identical current density range, the water content and the proton conductivity are linearly proportional to each other, showing that the lower water content, the higher the current density. Although the SSFFP, the IFFP and the SPFFP have almost identical water contents in the respective current density sections, the water content of the PFFP appears lower than other flow field patterns. In case of PFFP, as the reactants flow through a network of series and parallel flow paths only low pressure drops occur. However, this leads to inhomogeneous gas distribution or reactant maldistribution and locally flooding and heating phenomenon which result in the lowest membrane water content. An increase in the number of channels uniformly distributed the current density and temperature values under the ribs, compared to those values achieved under the channels. This behaviour increases the membrane water content due to reduction of saturation pressure of water, thus enhancing local performance and, therefore, the overall PEMFC performance [20].
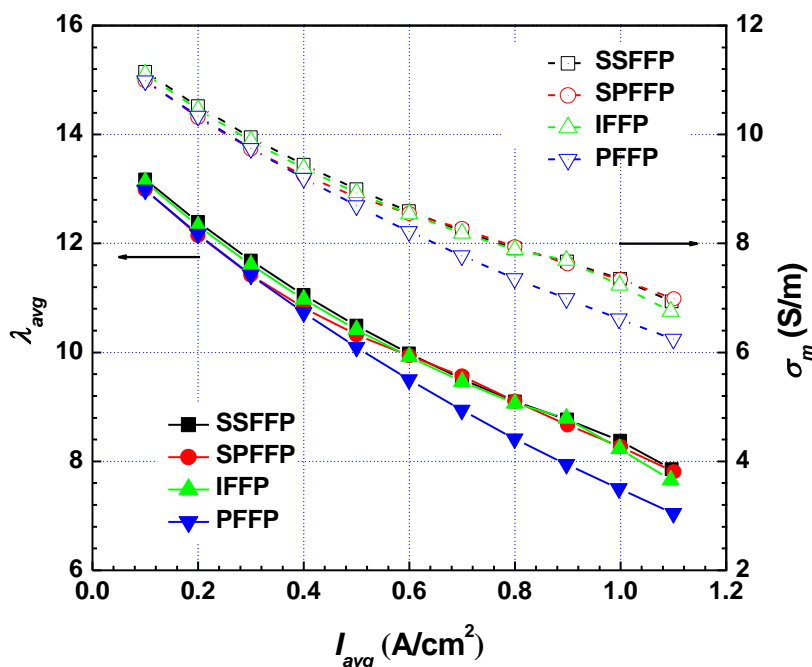
Figure 5. Average water content of membrane (λ_{avg} ; solid symbol) and average membrane conductivity (σ_m; hollow symbol) at each point on performance curves of four different flow field patterns.

In Fig. 5, the proportional linear relationship of the membrane conductivity mentioned above and the fact of the maximum water content ($\lambda_{max} = 14$) are well noticeable. Therefore, it is assumed that the flooding phenomenon takes place inside the channel. The water content plays a role in reducing the internal resistance of the membrane when high water content is related to high conductivity. In this analysis model, when the maximum water content is 14, the membrane conductivity has its maximum value of 12. Also, since the flooding phenomenon is related to the performance degradation because of the stagnant water existing inside the channel, the reduction of membrane conductivity does not occur. All the configurations show that average water content of membrane is under 14, thus the water flooding is predicted not to be significant for all flow-field configurations. This is closely linked to temperature and humidity conditions [18].

Fig. 6 shows the average net water flux per proton and the average membrane water content in the respective current density sections. Water balance on the anode and cathode is one of very important factors in terms of fuel cell water management, which is primarily associated with the membrane water content and the net water flux per proton. Fig. 6 illustrates how average net water flux per proton and average membrane water content change as the average current density increases. The water concentration gradient inside the channel and the pressure difference between anode and cathode generate water behavior, while the water content of membrane changes net water flux per proton.
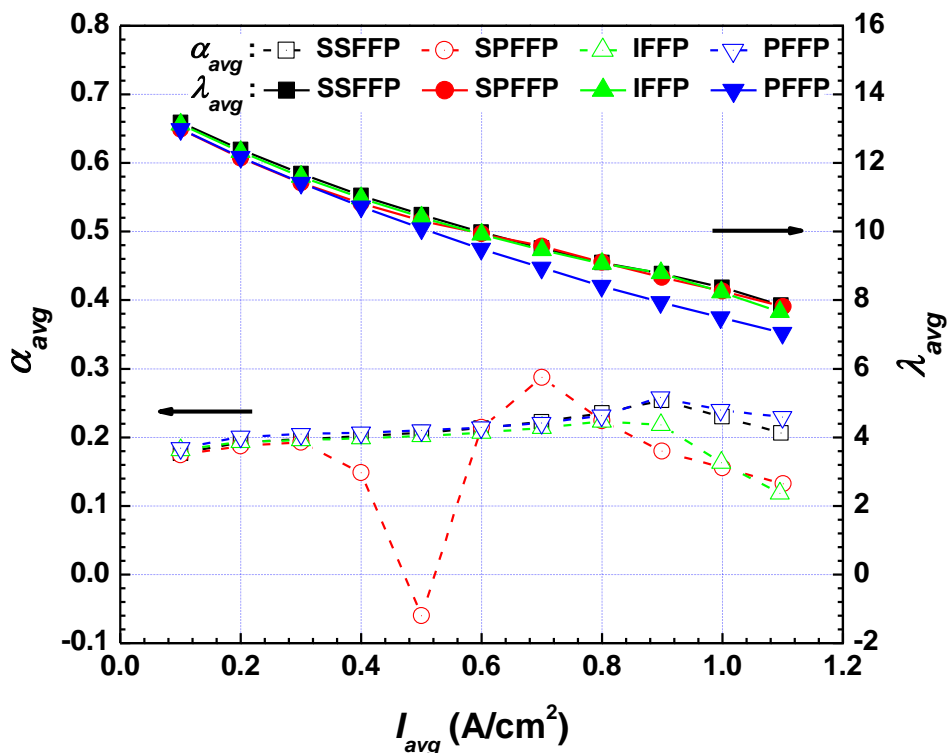
Figure 6. Average net water flux per proton (α_{avg}; hollow symbol) and average water content of membrane (λ_{avg}; solid symbol) at each point on performance curves of four different flow field patterns.

The net water flux per proton, which expresses the water transport between anode and cathode, is affected by the electro-osmotic drag coefficient (η_d) as a function of the membrane water content as follows [15,18]:

$$\eta_d = 0.029\lambda^2 + 0.05\lambda - 3.4 \times 10^{-19} \tag{4}$$

$$\alpha = \eta_d - \frac{F}{I(x,y)} D_w \frac{(C_{w,c} - C_{w,a})}{t_m} \tag{5}$$

Where $I(x,y)$ is the local current density in A/m^2, $C_{w,c}$ and $C_{w,a}$ is the concentration of water vapor at the anode and the cathode in mol/m^3, respectively. If the net water flux per proton is greater than 0, the electro-osmotic drag is higher than back diffusion, and the water is transported from the anode to the cathode. On the other hand, the net water flux per proton is less than 0 mainly in the outlet area under the ribs, and the water is transported from the cathode to the anode by back diffusion.

In case of a flow field pattern that has difficulty in water removal in the section of a high current density, the average net water flux per proton decreases. Particularly, the IFFP and the SPFFP see the net water flux per proton drop in the section where I_{avg} = 0.9~1.1 A/cm^2. In case of the SPFFP with poor features of water removal and pressure distribution due to the flow imbalance as shown in Fig. 3 (b), the water behavior is most unstable in the section where I_{avg} = 0.4~1.1 A/cm^2 and it drops to the point that α = -2.25 where back diffusions occur at the section of I_{avg} = 0.5 A/cm^2. Where I_{avg} = 0.5 and 0.7 A/cm^2, the net water flux per proton takes a sudden turn, which agrees with the difficulty in water removal due to flow imbalance. Krandlikar et al. [27] studied theoretically and experimentally of flow maldistribution in a four-tube parallel channel geometry. The maldistribution in SPFFP may be caused, among others, by uneven flow resistances in the parallel channels caused by variations in channel dimensions, different flow lengths, uneven fouling, density and viscosity variations, and presence of two or more phases due to water content in the channels.

3.5 Current density distribution

Cell performance is often described by the polarization curve, i.e., cell voltage *versus* current density. The polarization curves of the PEMFC that has four flow field patterns were calculated and classified into three categories of an activation loss region, an ohmic resistance loss region, and a mass transport loss region as shown in Fig. 7. In this curve, three main polarization loss regions could be identified: (i) activation loss region ranged between the cell voltages of 0.980 V and 0.767 V; (ii) ohmic resistance loss region ranged between the cell voltages of 0.762 V and 0.466 V; and (iii) mass transport loss region ranged between the cell voltages of 0.440 V and 0.333 V. The activation loss regions of the four flow field patterns are almost identical; however, the cell voltage of the SPFFP is a sharp drop from the ohmic resistance loss region and the mass transport loss region does not exist. This can be explained by the water flooding due to deficient water removal and the uneven distributions of the reactants, as shown in Figs. 3 and 6. In general maldistribution in parallel channels may be caused, among others, by uneven flow resistances in the parallel channels caused by variations in channel

dimensions, different flow lengths, uneven fouling, density and viscosity variations, and presence of two or more phases due to water content in the channels [27]. The mass transport loss region of the PFFP, which has a smaller cell voltage, is probably caused by hydrating membranes due to excessive water removal at the outlet. The pin-type flow field consist of columnar pins arranged in a regular pattern. As the reactants flow through a network of series and parallel flow paths only low pressure drops occur. However, this leads to inhomogeneous gas distribution or reactant maldistribution and locally flooding and heating phenomenon [20].
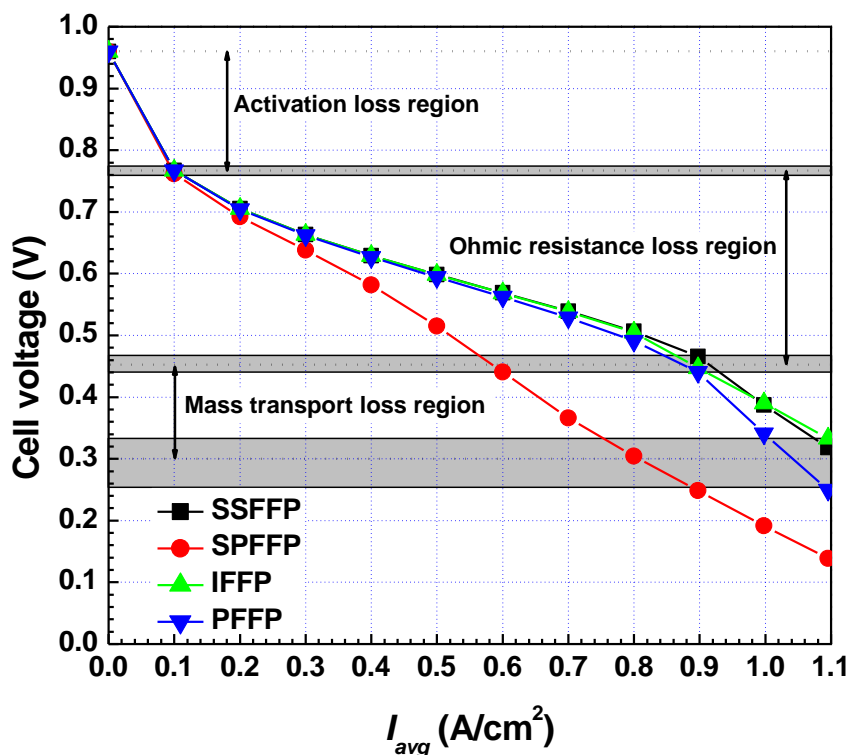
Figure 7. The polarization curves of four different flow field patterns at 1.5 / 2.0 stoichiometric number under the conditions of 101 kPa system pressure and 75 °C cell temperature.

Fig. 8 represents the current density distributions at the MEA surface on the SSFFP, the SPFFP, the IFFP and the PFFP. The SSFFP shows the highest cell voltage in comparisons with other flow field patterns. The cell voltages of the SSFFP, the SPFFP, the IFFP and the PFFP are 0.5689, 0.4404, 0.5685, and 0.5622 V at I_{avg}=0.6 A/cm^2, respectively. On the other hand, Kumar et al. [28] presented the simulation results that serpentine, parallel, multi-parallel and discontinuous flow channels were analysed at PEMFC voltage values of 0.66, 0.64, 0.68 and 0.71 V at I_{avg}=0.5 A/cm^2, respectively to study the steady and transient behaviour of the PEM fuel cell. This work shows that in a steady state PEMFC performance the discontinuous design will perform better than the other three designs. The reason is that the discontinuity of the channels forced the gas into the GDL, thus converting the transfer of reactant through the GDL from diffusion to diffusion and convective, and thereby, increasing the local effective pressure of reactant at the reaction interface. However, it was

found that the best PEMFC performance in transient response was for the parallel flow field design, showing the lower performance in a steady-state conduct. Therefore, this difference of the cell voltage may be attributed to BP flow field and configuration, operating conditions and steady-state and transient.

The current density is locally high mainly at the rib part due to the under-rib convection, and changes by the factors such as water concentration, membrane conductivity and temperature. The uniformity of current density becomes an important to verify the life time and lead to the durability of PEMFC. The current density distribution of the SPFFP is considerably more non-uniform than those of the other flow field patterns. The straight parallel version is the simplest one requiring the smallest pressure drop by equally distributing the flow rate into many parallel paths. However, if the flow resistance is not maintained at the same level in each parallel flow channel a non-uniform distribution of the reactants may occur [29].

(a) SSFFP   (b) SPFFP

(C) IFFP   (d) PFFP
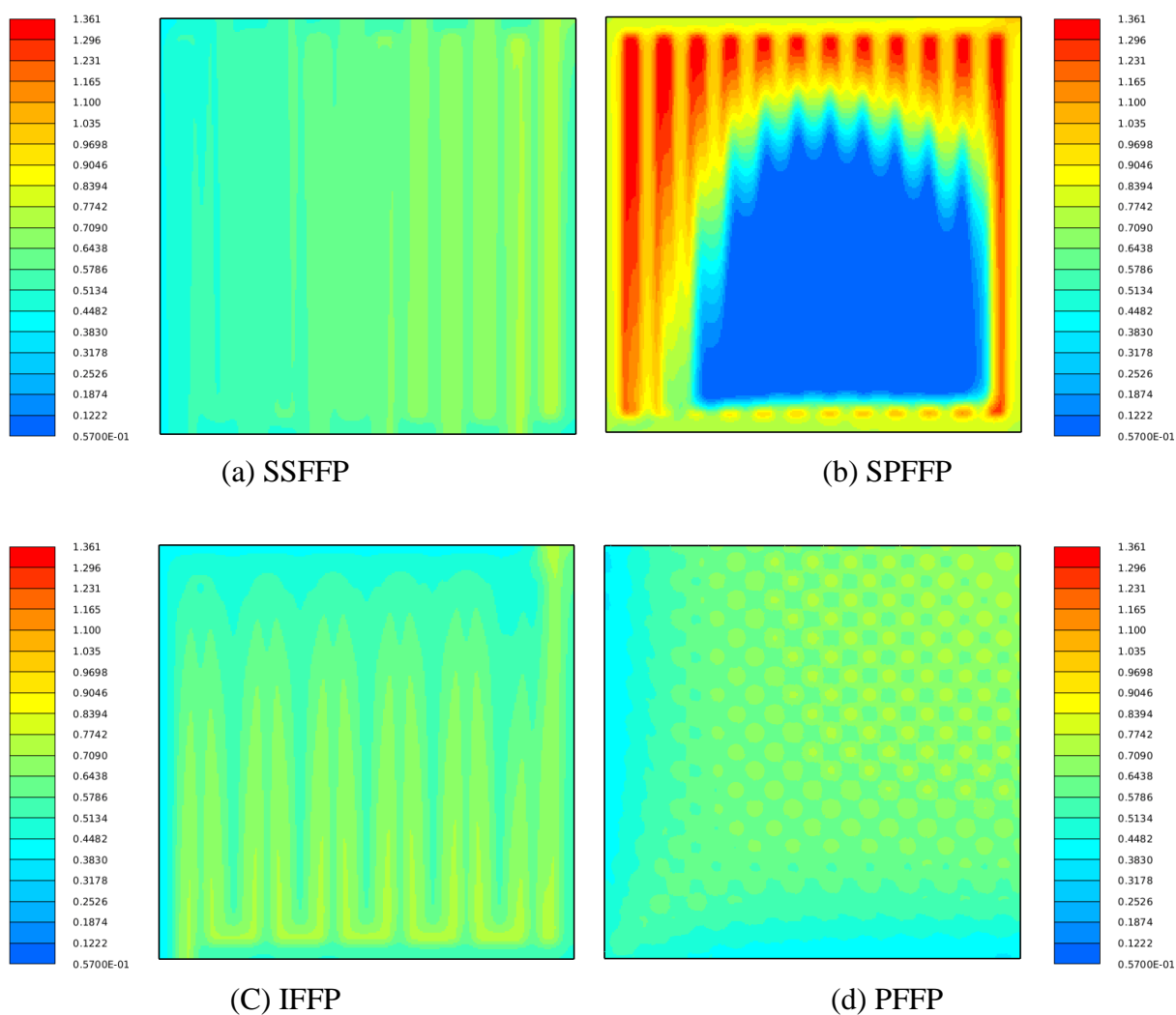
Figure 8. Comparison of the current density distribution contours between the four different flow field patterns at $I_{avg} = 0.6$ A/cm^2.

4. CONCLUSIONS

In this study, the numerical optimization of flow field pattern was performed by the mass transfer and electrochemical reaction characteristics prior to the experiment in PEMFC. We analyzed the four flow field patterns numerically and the results led us to draw the following conclusions. When the active areas and operating conditions are identical, the SSFFP showed the best mass transfer characteristics or mass transfer characteristics similar to the interdigitated flow field pattern which shows that the water accumulated because of the electrochemical reaction in the outlet region. In the IFFP, water content increases in the section of high current density, and the water behavior becomes unstable at the outlet channels. In the PFFP, excessive water removal results in dehydration of the membrane, whereas in the SPFFP, flooding occurs because of uneven flow circulation. The numerical optimization of flow field pattern incorporates mass transfer and electrochemical reaction characteristics to give qualitative assessments of pressure, flow, water and current density prior to experiment.

References

1. S. M. Haile, D. A. Boysen, C. R. I. Chisholm and R. B. Merle, *Nature*, 410 (2001) 910.
2. S. Tsushima and S. Hirai, *Prog. Energy Combust. Sci.*, 37 (2011) 204.
3. H.-M. Kim, *Nature*, 477 (2011) 280.
4. H. Presting and U. König, *Mater. Sci. Eng. C*, 23 (2003) 737.
5. M. Y. El-Sharkh, A. Rahman and M. S. Alam, *Int. J. Hydrog. Energy*, 35 (2010) 11099.
6. Y. Sone, *J. Power Sources*, 196 (2011) 9076.
7. C. M. Bautista-Rodríguez, A. Rosas-Paleta, A. Rodríguez-Castellanos, J. A. Rivera-Márquez, O. Solorza-Feria, J. A. Guevara-Garcia and J. I. Castillo-Velázquez, *Int. J. Electrochem. Sci.*, 2 (2007) 820.
8. X. D. Wang, X. X. Zhang, W. M. Yan, D. J. Lee and A. Su, *Int. J. Hydrog. Energy*, 34 (2009) 3823.
9. X. D. Wang, J. L. Xu, W. M. Yan, D. J. Lee and A. Su, *Int. J. Heat. Mass Tran.*, 54 (2011) 2375.
10. Lee H., Lee C., Oh T., Choi S., Park I. and Baek K., *J. Power Sources*, 107 (2002) 110.
11. M. Khoeiniha and H. Zarabadipour, *Int. J. Electrochem. Sci.*, 7 (2012) 6302.
12. T. V. Nguyen and R. E. White, *J. Electrochem Soc.*, 140 (1993) 2178.
13. S. W. Cha, R. O'Hayre, Y. Saito and F. B. Prinz, *J. Power Sources*, 134 (2004) 57.
14. K. B. Shyam Prasad, P. V. Suresh and S. Jayanti, *Int. J. Hydrog. Energy*, 34 (2009) 8289.
15. K.-S. Choi, H.-M. Kim and S.-M. Moon, *Int. J. Hydrog. Energy*, 36 (2011) 1613.
16. K.-S. Choi, H.-M. Kim and S.-M. Moon, *Electrochem. Commun.*, 13 (2011) 1387.
17. K.-S. Choi, B.-G. Kim, K. Park and H.-M. Kim, *Comput. Fluids*, 69 (2012) 81.
18. D. H. Jeon, S. Greenway, S. Shimpalee and J. W. Van Zee, *Int. J. Hydrog. Energy*, 33 (2008) 1052.
19. J. Larminie and A. Dicks, *Fuel Cell Systems Explained*, John Wiley and Sons Ltd., London (2003).

20. A. P. Manso, F. F. Marzo, J. Barranco, X. Garikano and M. Garmendia Mujika, *Int. J. Hydrog. Energy*, 37 (2012) 15256.
21. J. H. Nam, K.-J. Lee, S. Sohn and C.-H. Kim, *J. Power Sources*, 188 (2009) 14.
22. J.-H. Jang, W.-M. Yan, H.-Y. Li and W.-C. Tsai, *Int. J. Hydrog. Energy*, 33 (2008) 156.
23. J.-J. Hwang and H.-S. Hwang, *J. Power Sources*, 104 (2009) 24.
24. T. E. Springer, T. A. Zawodzinski and S. Gottesfeld, *J. Electrochem Soc.*, 138 (1991) 2334.
25. T. A. Zawodzinski, T. Springer, F. Uribe and S. Gottesfeld, *Solid State Ionics*, 60 (1993) 199.
26. T. Fuller and J. Newman, *J. Electrochem Soc.*, 139 (1992) 1332.
27. S. G. Kandlikar, Z. Lu, W. E. Domigan, A. D. White and M. W. Benedict, *Int. J. Heat. Mass Tran.*, 52 (2009) 1741.
28. A. Kumar and R. G. Reddy, *J. Power Sources*, 155 (2006) 264.
29. X. Li and I. Sabir, *Int. J. Hydrog. Energy*, 30 (2005) 359.